The Separated Polar Winter Stratopause: A Gravity Wave Driven Climatological Feature

MATTHEW H. HITCHMAN,* JOHN C. GILLE, CLIVE D. RODGERS,† AND GUY BRASSEUR

National Center for Atmospheric Research,‡ Boulder, Colorado

(Manuscript received 12 April 1988, in final form 22 August 1988)

ABSTRACT

An examination of satellite-derived temperatures reveals that the winter polar stratopause is usually elevated and warmer than the adjacent midlatitude stratopause. This "separated stratopause" occurs in both hemispheres, but is more pronounced and persistent in the southern winter. It descends with time towards spring and exhibits week to week variability. Observational diagnostics and results from a two-dimensional (2-D) model suggest that gravity wave driving can account for this separated polar stratopause by driving a meridional circulation, with downwelling over the winter pole. In the model, the solar heating pattern induces stronger winter westerlies than summer easterlies, which leads to a stronger gravity wave driven circulation in the winter hemisphere. Spherical geometry and the high latitude location of the winter westerly jet combine to yield a concentrated region of downwelling. Model results suggest that descent of the temperature maximum with time is probably caused by wave–mean flow interaction.

1. Introduction

The earth's stratopause, a feature unique in our solar system, owes its existence to absorption of ultraviolet radiation by ozone. One might expect from radiative arguments alone that stratopause temperatures should descrease going from the sunlit summer toward the dark winter pole. It was, therefore, quite surprising when Barnett (1974) reported that during the southern winter and spring of 1971, stratopause temperatures reached a relative *maximum* over the south pole. Figure 1, taken from his paper, shows temperatures derived from channel A of the Nimbus-4 selective chopper radiometer (SCR), which has a weighting function peaking near 45 km, just below the stratopause. Aside from the event in early January, temperatures during the northern winters decreased monotonically toward the north pole (Fig. 1). In contrast, during the southern winter 1971, the pole began to warm relative to midlatitudes beginning in June. By the end of September the warmest air at 2 mb was to be found at the south pole (>270 K), more than 20 K warmer than at 50°S.

Since the Nimbus 4 SCR instrument, other satellite instruments have provided data to higher altitudes or with better vertical resolution. Data taken by the Nimbus-6 pressure modulator radiometer (PMR) cover the region 80°S–80°N, ~20–90 km, with a resolution of ~15 km. Data from the Nimbus-7 Limb Infrared Monitor of the Stratosphere (LIMS) cover the region 64°S–84°N, ~15–70 km, with a ~3 km vertical resolution. The PMR and LIMS data are described in section 2. We use the portion of the PMR temperature dataset for June 23, 1975–January 6, 1976, which has recently been reprocessed using improved inversion and mapping algorithms, and the LIMS data set, covering the period 25 October 1978–28 May 1979, to document the structure and behavior of the winter stratopause (section 3). In early winter a distinct region of high temperatures forms in the polar mesosphere and descends with time. This climatological feature occurs in both hemispheres. We will refer to it as the "separated stratopause." It is part of a deep global pattern which includes the reversed latitudinal temperature gradient near the mesopause. To facilitate interpretation of the analysis, in section 4 we describe several mechanisms which follow from the theory that gravity-wave driving can account for this structure.

The high vertical resolution of the LIMS data allows accurate estimates of radiative heating rates and residual mean meridional circulations to be made. Together with the planetary wave fluxes determined from LIMS temperatures, the angular momentum budget can be calculated. In section 5 we use late November 1978 as a representative time from the LIMS data record to diagnose the cause of the separated winter stratopause. Large radiative cooling rates are found in a deep layer

* Present affiliation: Meteorology Department, University of Wisconsin-Madison.

† Permanent affiliation: Department of Atmospheric Physics, University of Oxford, United Kingdom.

‡ The National Center for Atmospheric Research is sponsored by the National Science Foundation.

Corresponding author address: Dr. Matthew H. Hitchman, Meteorology Department, University of Wisconsin-Madison, Madison, WI 53706.

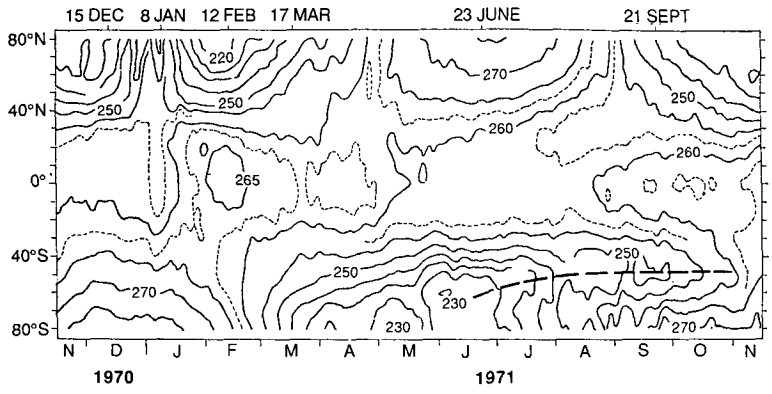

FIG. 1. Latitude–time section of zonal mean temperature for channel A of the Nimbus-4 Selective Chopper Radiometer, taken from Fig. 2a of Barnett (1974). The period covered is 16 November 1970–15 November 1971. The contour interval is 5 K. The heavy dashed line is a locus of minimum temperature.

over the winter pole, suggesting that dynamical heating is required to account for this phenomenon. The pattern of the residual in the angular momentum budget agrees well with that for the zonal body force obtained from Lindzen's (1981) parameterization of breaking gravity waves using LIMS zonal winds. These calculations support the hypothesis that gravity wave absorption induces a mesospheric flow toward the winter pole, with the descending branch of the circulation bringing high entropy air downward over the pole in a confined region. This downward advection maintains elevated temperatures against radiation to space.

To test the gravity wave driving hypothesis further we employed a two-dimensional (2-D) numerical model of the middle atmosphere. In section 6 we compare two runs of the BISA/NCAR model. In run 1, no friction or small-scale wave driving was allowed. In run 2, we employed Lindzen's gravity-wave parameterization, as modified by Holton (1982) for use in models. We will refer to this as the L/H parameterization. These mechanistic calculations support the idea that gravity waves control the shape and strength of the polar winter stratopause.

2. Data and analysis

a. Nimbus-6 PMR temperatures

The PMR instrument has been described by Curtis et al. (1974), and results have been reported by Hirota and Barnett (1977) and Crane (1979), among others. The PMR data are essential for describing the separated winter stratopause because they include the upper stratosphere and entire mesosphere, and extend nearly to the poles. Barnett and Corney's (1985) middle atmosphere climatology is based primarily on the PMR data. They employed 3 years of PMR data (June 1975–July 1978), using the method of Rodgers (1976) to retrieve monthly mean temperatures at each grid point in the meridional plane. Daily zonal mean temperature cross sections have been developed for the period 23 June 1975–6 January 1976, using improved inversion and mapping algorithms, which will be described elsewhere. The highest altitude weighting function peaks at about 80 km. Although departures from local thermodynamic equilibrium were taken into account, caution should be used in interpreting anything except the broadest, most coherent features in the upper mesosphere. There is very little independent information below 30 km.

b. LIMS temperatures and heating rates

The LIMS experiment has been described by Gille and Russell (1984). Absolute temperature accuracy is better than 2 K, while precision is better than 0.6 K, in the pressure range 100–1 mb (Gille et al. 1984). Mapped version-4 temperature fields are used. The inversion algorithm is described in Bailey and Gille (1986), and the v4 mapped data qualities are described in Hitchman and Leovy (1986; hereafter HL). The determination of zonal winds, radiative heating rates using the algorithm of Wehrbein and Leovy (1982), and resulting meridional circulations, are described in sections 3 and 5 of HL, except for an example of solar heating rates calculated as in Gille and Lyjak (1986). The magnitude of the residual circulation is quite comparable to other observational estimates (Crane et al. 1980; Solomon et al. 1986; Gille et al. 1987) and results from numerical models (e.g., Holton 1983). It proved to be convenient to use 6 day means for calculating the angular momentum budget, since there are 36 such periods in the 216 day record.

c. Two estimates of gravity wave driving

"Advective" eddy wind components and the body force due to quasi-stationary planetary scale waves,

DF_p, are determined as in Hitchman et al. (1987). Once zonal winds, $\bar{u}$, the transformed Eulerian mean meridional circulation (Edmon et al. 1980), $(\bar{v}^*, \bar{w}^*)$, and DF_p are known, an estimate of the required zonal body force due to waves unresolved by the LIMS instrument can be made from the residual in the zonal momentum equation:

$$DF_{\text{res}} = \frac{\partial \bar{u}}{\partial t} + \bar{w}^* \frac{\partial \bar{u}}{\partial z} + \bar{v}^* \left(\frac{\partial \bar{u}}{\partial y} - f \right) - DF_p. \quad (1)$$

A separate estimate of wave driving due to breaking gravity waves may be made with the L/H parameterization. Gravity waves will break when their amplitudes are so large that they become convectively unstable. The mean zonal flow will accelerate toward the zonal trace speed c (Pedlosky 1979, p. 72) of the wave in the region above the breaking level, z_b, where eddy zonal wind amplitude is comparable to the intrinsic zonal trace speed ($|u'| = |c - \bar{u}|$), and below the critical level, z_c, where $c = \bar{u}$. In this region, wave amplitudes are assumed to cease their exponential growth with altitude and are reduced to a constant amplitude profile by convective turbulence. Waves transfer momentum from the troposphere to the local mean flow at the rate

$$DF_g = A(c - \bar{u})^2 \left[(c - \bar{u}) + 3H \frac{\partial \bar{u}}{\partial z} \right] \quad (2)$$

in the range $z_b \leq z \leq z_c$, where

$$z_b = 3H \ln \left[\frac{|c - \bar{u}|}{\tilde{u}} \right]. \quad (3)$$

Zonal mean wind profiles used in (2) and (3) are calculated from LIMS observations. The Coriolis parameter is f, while H is the scale height. Zonal trace speeds and the parameters A and $\tilde{u}$, which represent wave properties at 15 km, are specified in Table 1. Unsteady flow over topography or convection will excite a gravity wave packet, necessarily comprising a spectrum of phase speeds. The values of $\tilde{u}$ and A were changed from Holton's (1983) values to provide better agreement between DF_g and DF_{res} for mid-December 1978. The algorithm then was applied at all times. Profiles of DF_g were smoothed in the vertical to approximate various effects such as nonlinear interaction among waves and radiative damping.

Patterns resulting from (1) and (2) have been shown to be similar in a study of the momentum budget of the equatorial stratopause semiannual oscillation (SAO) (Hitchman and Leovy 1988).

3. Winter stratopause structure

To document the structure of the stratopause we show two sequences of zonal mean temperature sections, each panel spaced a month apart. Progressing counterclockwise from the upper left in Fig. 2 one sees the evolution of PMR middle atmosphere temperatures from the June solstice through the December solstice in 1975. By arranging the panels in this fashion, the near symmetry about the equinox can be seen. Aside from the winter polar regions, at each latitude, temperatures maximize near 45–50 km altitude, forming the stratopause. At the solstices, temperatures decrease monotonically along the stratopause toward the winter pole, with a minimum being reached near 50° in the winter hemisphere. Then a large warm anomaly is encountered. On 30 June this warm region was centered near 60 km, 65°S. It descended with time through 30 September, after which it became less distinct. In the Northern Hemisphere after 30 September, a new elevated separate warm region began to form. By 30 December the temperature maximum was located near 55 km, 65°N.

In the mesosphere the latitudinal temperature gradient is "reversed" at the solstices, in the sense that temperatures decrease toward the summer pole, opposite to what would be expected from simple local radiative budgets. Figure 2 shows the spatial relationship between the warm summer stratopause, cold summer mesopause, and separated winter stratopause. The separated stratopause is a central feature to examine for understanding this pattern. It is thought that the "reversed" mesospheric temperature gradient is due to gravity wave driving (Houghton 1978; Holton 1983). We pursue this as an explanation of the separated stratopause in section 4.

The LIMS data lack the high altitude and high southern latitude coverage of the PMR data, but have a much better vertical resolution. Progressing counterclockwise in Fig. 3, one sees the evolution of LIMS temperatures from late October through late May. The two sequences in Figs. 2 and 3 cover complementary parts of the annual cycle. The northern separated stratopause of October 1978 appeared to strengthen into November, contract in December, and disappear by February. Despite increased solar heating, high northern latitudes were cooler in February than in January.

The equatorial lower mesosphere was disturbed by a warm anomaly which appeared in December and descended to ~35 km by May. Descent of the SAO warm anomaly through the stratopause level in February and September can also be seen in Fig. 1. The warm anomaly was flanked by midlatitude cold anomalies, the pattern expanding in latitude as it descended (HL). The apparent contraction of the polar warm feature in December is partly due to this strong midlatitude upwelling and cooling associated with the SAO. In March and April the flanking cool regions were near the stratopause (Fig. 3).

Figures 1, 2 and 3 suggest that, during a given winter, the Southern Hemisphere separated stratopause is less variable, more robust, and longer lasting than its northern winter counterpart. The northern feature is not very noticeable below 45 km. This is compatible with Barnett's finding that a warm winter pole was

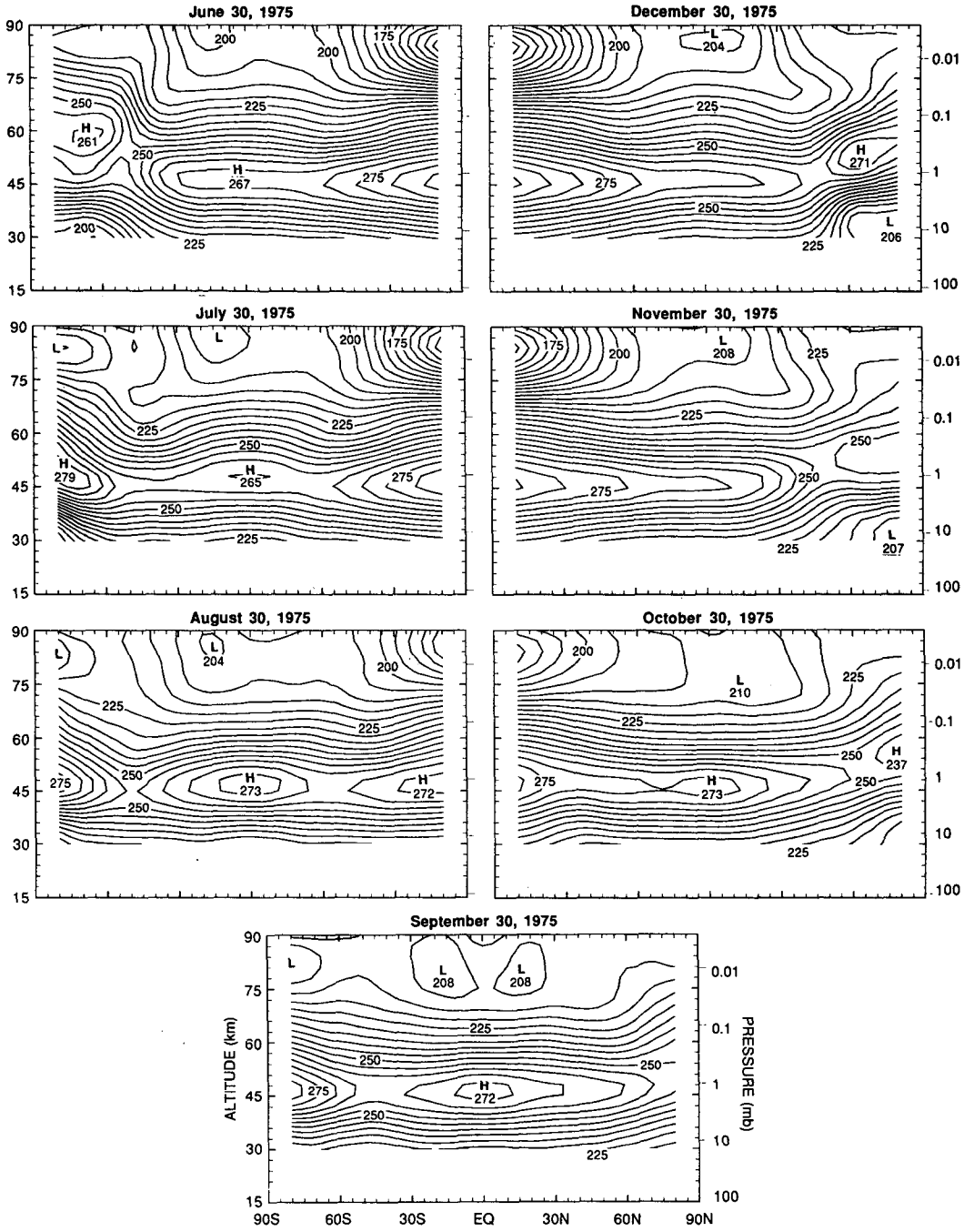

FIG. 2. Latitude–height sections of zonal mean temperature from the Nimbus-6 PMR instrument. The 30th of each month from June to December 1975 is shown, starting in the upper left, going counterclockwise. The contour interval is 5 K.

seen in channel A only in the southern winter during 1970–1971. By examining Figs. 1 and 2, one can see that at 45 km the temperature minimum near 50°S had already formed by late June in both 1971 and 1975, and became increasingly pronounced as the warm region descended over the pole. The southern feature was still quite pronounced at the end of September 1975 (Fig. 2), while the northern feature in 1979 was gone by early February (Fig. 3).

There is also a suggestion of greater interannual variability among northern winters. During October, November and December the northern feature behaved differently during 1975 and 1978. The southern separated stratopause of May 1979, however, was quite

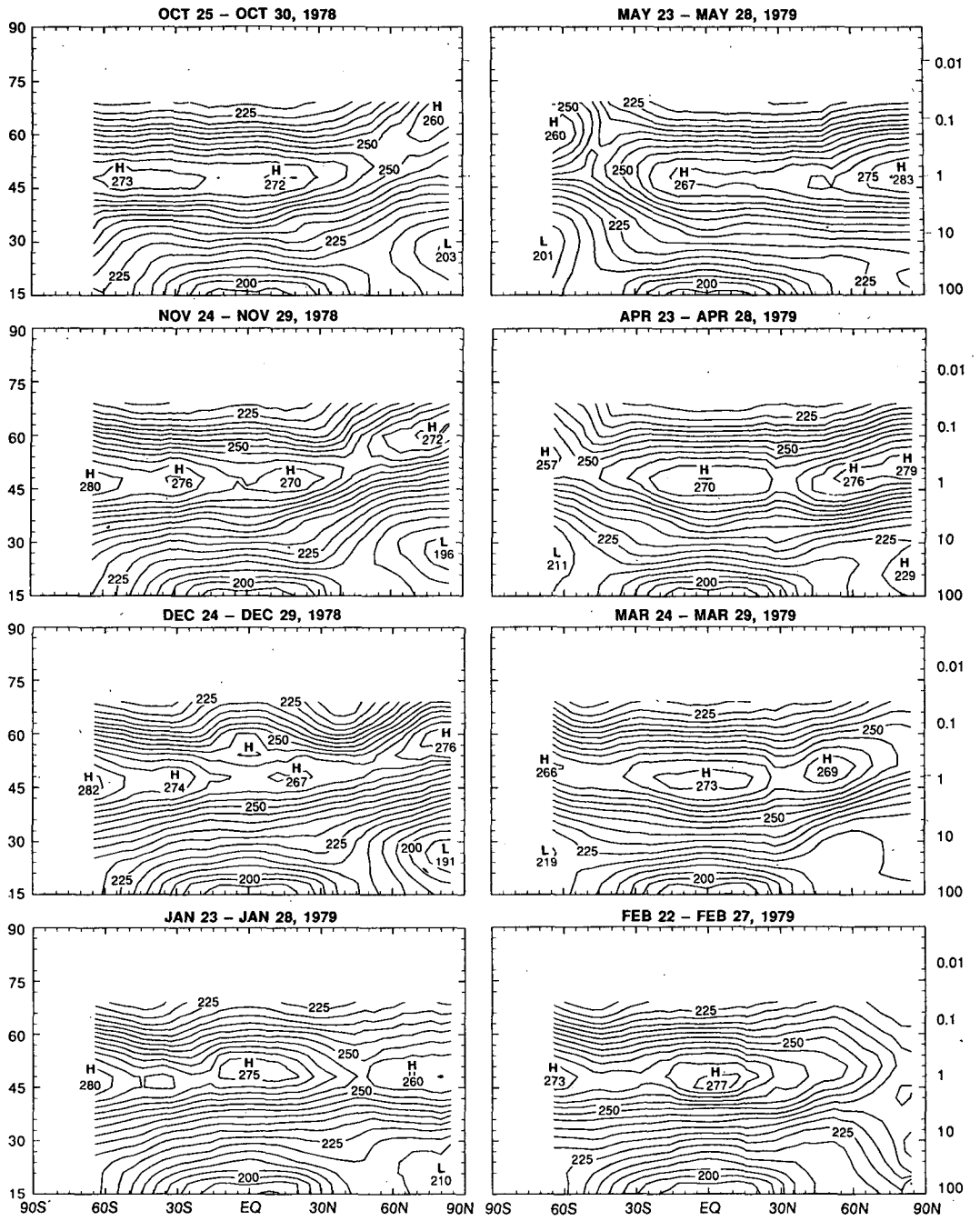

FIG. 3. Latitude–height sections of zonal mean temperature from the Nimbus-7 LIMS instrument. Six-day means near the end of each month from October 1978 to May 1979 are shown, starting in the upper left, going counterclockwise. The contour interval is 5 K.

similar in appearance to that of June 1975, including the altitude of the temperature maximum and the strikingly strong equatorward temperature decrease near 50°S.

To further evaluate interhemispheric differences in the morphology of the separated stratopause we examined the climatological charts which appear in MAP Handbook 16 (Barnett and Corney 1985). These multiyear average statistics verify that the Southern Hemisphere separated stratopause is distinctively stronger and steadier than that during the northern winter. Indeed, according to Barnett and Corney: "The temper-

ature maximum at the stratopause in July at 80°S is very much warmer than that for the Northern Hemisphere 6 months later."

The stratopause over the winter pole behaves differently than the sunlit stratopause. It is an isolated temperature maximum, which has a vertical extent of about four scale heights. This pattern can be produced simply by dynamically driven descent over the winter pole. The separated stratopause exhibits week to week variability. Such variability can be seen in Fig. 12 of HL during winter in both hemispheres. This suggests that a variable and rapid process is responsible for the separated stratopause, implicating wave–mean flow interaction, rather than differential radiative heating, as the operative mechanism.

4. The gravity-wave driving hypothesis

The reversed meridional temperature gradient near the solstices in Figs. 2 and 3 shows that mesospheric temperatures are not radiatively controlled. Haurwitz (1961) was the first to recognize that a frictionally induced meridional circulation is required to obtain this structure. It is now believed that gravity wave driving accomplishes the required "friction." Although Eqs. (2) and (3), together with the discrete parameters in Table 1, are clearly an approximation to rather complex processes, these relations capture the essential physics of gravity wave–mean flow interaction in the middle atmosphere. Several broad properties may be anticipated from theory.

Due to the dependence of z_b on $|c - \bar{u}|$ in (3), waves of opposing trace speed will break at much different altitudes. At a given level, DF_g will be controlled by waves traveling in one direction. In the extratropics the first term in brackets dominates in (2), so that $DF_g \approx (c - \bar{u})^3$, and the mean flow will accelerate toward the trace speed of the wave. In the winter westerly jet, westerly waves will break at low altitudes where $|c - \bar{u}|$ is small, causing a small westerly acceleration. At higher levels, where the easterly waves finally break, a large easterly acceleration will result. Thus, given the cubed dependence in (2), DF_g is expected to be largest in the jets and directed opposite to the zonal flow.

Approaching a solstice, differential radiative heating alone will give rise to a summer easterly jet and a winter westerly jet. It is reasonable to expect that the westerly jet will initially be stronger, due to the strong gradient in solar heating near the terminator. Thus, if the wave forcing is not strongly dependent on season, $|DF_g|$ will initially be larger in the winter hemisphere. Near the altitude of the jet maximum a transition occurs from a stratospheric regime, where the zonal flow is closer to its radiative equilibrium value, to a mesospheric regime, where the zonal flow is controlled by gravity-wave driving (Garcia and Solomon 1985). In the extratropical mesosphere the primary balance in the zonal momentum equation is

$$DF_g \approx -f\bar{v}^*. \tag{4}$$

In the winter hemisphere, an easterly body force ($DF_g < 0$) will induce a poleward flow (e.g., $\bar{v}^* > 0$ in the Northern Hemisphere). In the summer hemisphere a westerly body force ($DF_g > 0$) will induce an equatorward flow (e.g., $\bar{v}^* > 0$ in the Southern Hemisphere). Thus the pattern of gravity-wave driving gives rise to a continuous summer-to-winter meridional flow which is much stronger than the weak meridional drift which would occur in the absence of gravity waves (Holton 1983; Garcia and Solomon 1985).

Due to spherical geometry, this mesospheric flow will converge over the winter pole. Since this circulation is a strongly amplified version of a weak radiative circulation, ascent occurs in the summer hemisphere, with descent over the winter pole. The volume of radiatively cooled air in the polar night is smaller than that of the heated sunlit air. This difference may tend to produce a more confined region of descent. The strength of the mesospheric flow, however, is controlled by gravity-wave driving. It is expected that the high latitude location of the terminator, hence of the polar night jet, expected region of strong $|DF_g|$, and induced poleward flow, act to confine the region of strong subsidence warming over the winter pole, giving rise to a separated stratopause. Easterly acceleration on the upper side of the polar night jet would lead to a descent of the level of maximum westerlies, a progression which would be in geostrophic balance with the descending separated stratopause.

The effect of a strong gravity-wave driven meridional circulation on the temperature structure in the mesosphere may be seen in the thermodynamic energy equation in transformed Eulerian coordinates (Edmon et al. 1980). Below the mesopause it may be written, to a good approximation, as

$$\frac{\partial \bar{T}}{\partial t} + \bar{v}^* \frac{\partial \bar{T}}{\partial y} + \frac{\bar{T}N^2}{g}\bar{w}^* = \bar{Q}, \tag{5}$$

where N is buoyancy frequency, g acceleration due to gravity, and $\bar{Q}$ the net radiative heating rate. Near the mesopause an additional term involving a downward flux of entropy by breaking gravity waves becomes important (Coy and Fritts 1988). Throughout most of the atmosphere the vertical entropy gradient is quite

TABLE 1. Gravity wave parameters used with LIMS zonal winds. In the 2-D model, $\tilde{u} = 3$ m s^{-1} for all trace speeds.

c (m s^{-1})	A ($\times 10^{-9}$ s m^{-2})	$\tilde{u}$ (m s^{-1})
−40	0.5	1
−20	1.0	2
0	2.0	3
20	1.0	2
40	0.5	1

large, so that vertical advection is an efficient means of redistributing entropy. In a strong gravity-wave driving regime, angular momentum balance is maintained by induced meridional motions, as in (4). From continuity, vertical motions arise which dominate in (5). In the polar night, dynamically driven descent causes increased temperatures, which, in turn, causes much greater cooling to space. Over the sunlit summer pole, dynamically driven ascent advects low entropy air upward, causing decreased temperatures, leading to much greater net radiative heating. Dynamical heating is required to obtain the reversed meridional temperature gradient and separated stratopause, which can be accomplished by a gravity wave driven mean meridional circulation.

5. Observational diagnosis

A marked separated stratopause was present over the North Pole during 24–29 November 1978 (Fig. 3). We selected this period for detailed diagnostic studies using the LIMS data. The net solar heating for this period is shown in Fig. 4. Solar heating rates are largest over the summer pole. Near 50°N, the values drop off rapidly to zero in the northern pole night. In comparing the temperature and solar heating rate patterns for this period (Figs. 3, 4), southward of ~40°N in the sunlit region there is a very good correspondence in shape and altitude for the maximum. The stratopause structure in the winter high latitudes, however, cannot be explained by absorption of insolation by ozone. Since the largest meridional gradients of solar heating are near the winter pole, one might expect that early winter westerlies would be stronger than early summer easterlies. One would also expect the winter westerly jet to be located close to the terminator, and that, by the argument in section 4, large gravity wave driving would occur close to the pole.

Figure 5 shows the net radiative heating and residual mean meridional circulation for this period. Large

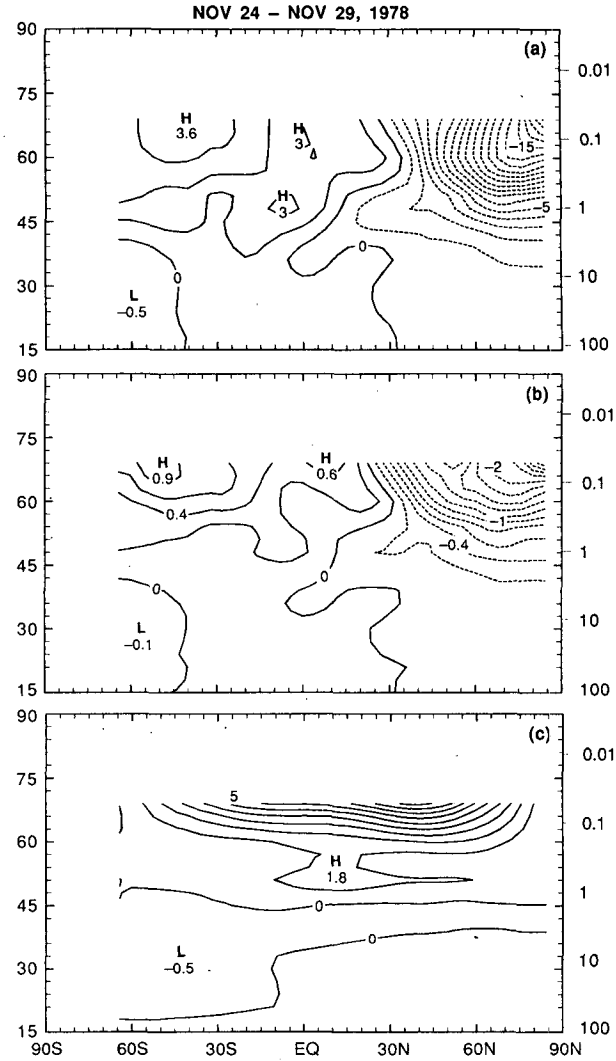

FIG. 5. Latitude–height sections of zonal mean (a) net heating rate, contour interval 1 K day^{-1}; (b) $\bar{w}^*$, contour interval 2 mm s^{-1}, and (c) $\bar{v}^*$, contour interval 1 m s^{-1}, for the period 24–29 November 1978.

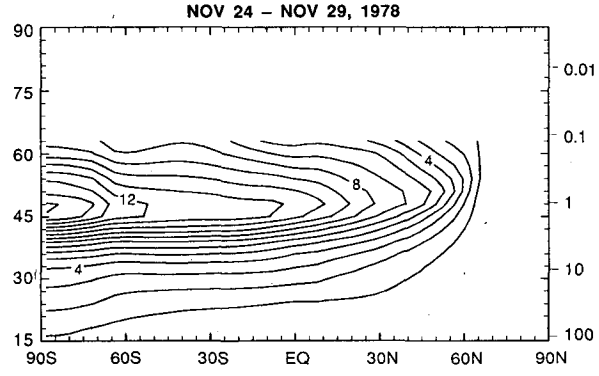

FIG. 4. Latitude–height section of zonal mean solar heating rate for the period 24–29 November 1978 calculated as described in Gille and Lyjak (1986). The contour interval is 1 K day^{-1}.

cooling rates are seen in the mesosphere poleward of ~40°N (Fig. 5a). This occurs in a region where solar heating is small and relaxation times are fairly short, yet temperatures are quite warm (Fig. 3). Patterns of net radiative heating largely reflect departures of the observed temperatures from radiative equilibrium. Some process other than radiation is maintaining the warm anomaly.

The residual mean meridional circulation required to maintain the observed temperature distribution against radiative damping is toward the winter pole and downward (Figs. 5c, b). The largest subsidence velocities (≈ -2 cm s^{-1}) occur just above the separated stratopause temperature maximum. Near 60 km, North Polar temperatures increased from October through December (Fig. 3). Since there is little solar

heating, these temperature increases must be caused by downwelling (cf. equation 5). Due to the strong vertical stratification of entropy, a moderate downward motion of 1 cm s^{-1} can cause heating at a rate of more than 10 K day^{-1}. This dynamically warmed region then cools to space at the rate seen in Fig. 5a. The temperature minimum near 50° in the winter hemisphere is simply the minimum between the sunlit stratopause and a warm polar anomaly caused by a global circulation with downwelling over the pole.

Ascent is typically weaker but is distributed over a broader region (Fig. 5b). Inspection of figures in Gille et al. (1987) reveals that this is also true of other near-solstice months. This seasonal asymmetry implies that dynamically driven departures from radiative equilibrium near the stratopause are smaller in the summer hemisphere. The relative confinement of downwelling air leads to stronger meridional temperature gradients and vertical wind shears in the winter mesosphere. As expected by the thermal wind law, the westerly jet closes off more rapidly with height than the summer easterly jet (Fig. 6a).

In the mesosphere, meridional advection of angular momentum usually dominates the other terms on the right-hand side of (1). The residual of these terms, DF_{res}, is shown in Fig. 6b. By (1) this pattern represents the acceleration due to waves which are too small and rapidly varying to be detected by LIMS. An independent calculation of gravity-wave driving based on the L/H parameterization (2) yields a similar pattern (Fig. 6c). We infer that in the mesosphere small-scale waves are responsible for deceleration of both the summer easterlies and the winter westerlies. Away from the equator, meridional motions have a component perpendicular to the axis of rotation, and are thus very efficient at advecting angular momentum. As described in section 4, at this time the positive torque in the Southern Hemisphere (Figs. 6b, c) is balanced by equatorward flow from high latitudes, closer to the axis of rotation, while the negative winter torque is balanced by poleward flow from low latitudes, which are far from the axis of rotation. This yields a continuous flow from the summer to winter pole, with descent over the winter pole (Fig. 5). Although the agreement between Figs. 6b and 6c is not perfect, this supports the concept that gravity wave absorption creates and maintains the separated stratopause, via a greatly strengthened meridional circulation.

The relationship between meridional motion and net radiative heating rates in the lower mesosphere is shown in Fig. 7. At 0.1 mb, the meridional flow strengthens much sooner in the winter hemisphere. This is also true of the southward flow in May. In both November and May, winter westerlies tend to strengthen sooner than summer easterlies (HL). Stronger winter westerlies arise from the radiative tendency to create a strong gradient near the polar night. Following the discussion of section 4, gravity-wave

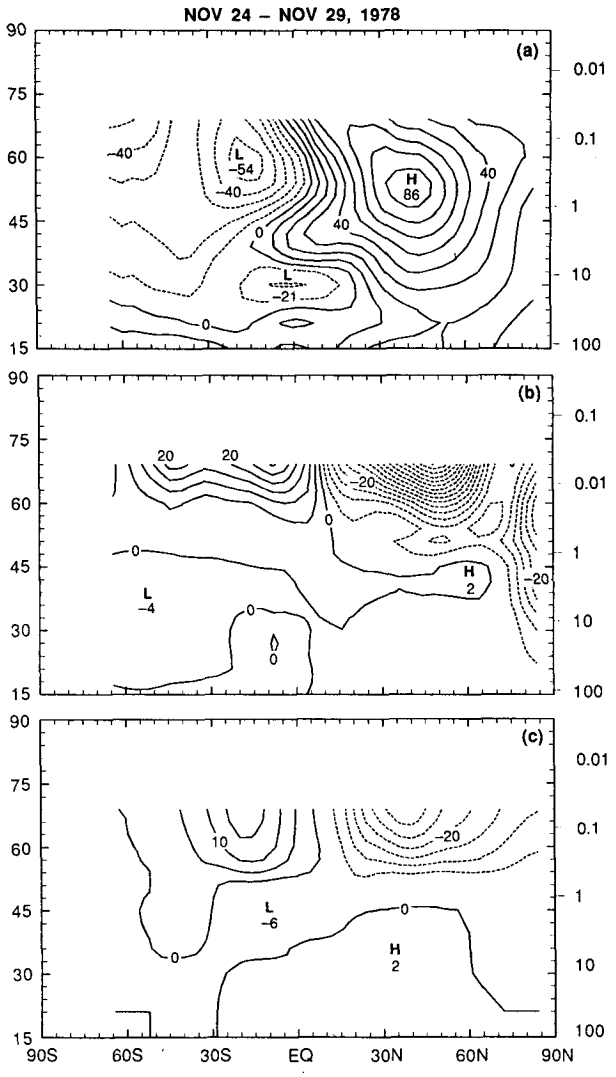

FIG. 6. As in Fig. 5, except of (a) zonal wind, contour interval 10 m s^{-1}; (b) DF_{res}, the residual in the LIMS momentum budget, and (c) DF_g, an estimate from the L/H parameterization. In (b) and (c) the contour interval is 5 m s^{-1} day^{-1}.

driving is strongest where zonal winds are strongest. Thus, the winter meridional circulation accelerates first.

Prior to March the flow is northward, being most rapid near 20°S and 50°N. The strong meridional convergence north of 50°N at this and higher altitudes (Fig. 7a) implies strong subsidence heating, hence strong infrared cooling at this level (Fig. 7b). The moderate meridional divergence south of 20°S (Fig. 7a) implies ascent, hence moderate radiative heating near 40°S (Fig. 7b). During December–January at 0.1 mb, radiative heating is enhanced in the subtropics, while there is cooling over the equator (Fig. 7b). This is caused by equatorial subsidence and midlatitude ascent associated with the SAO (HL).

Inferred winter downwelling appears to be stronger

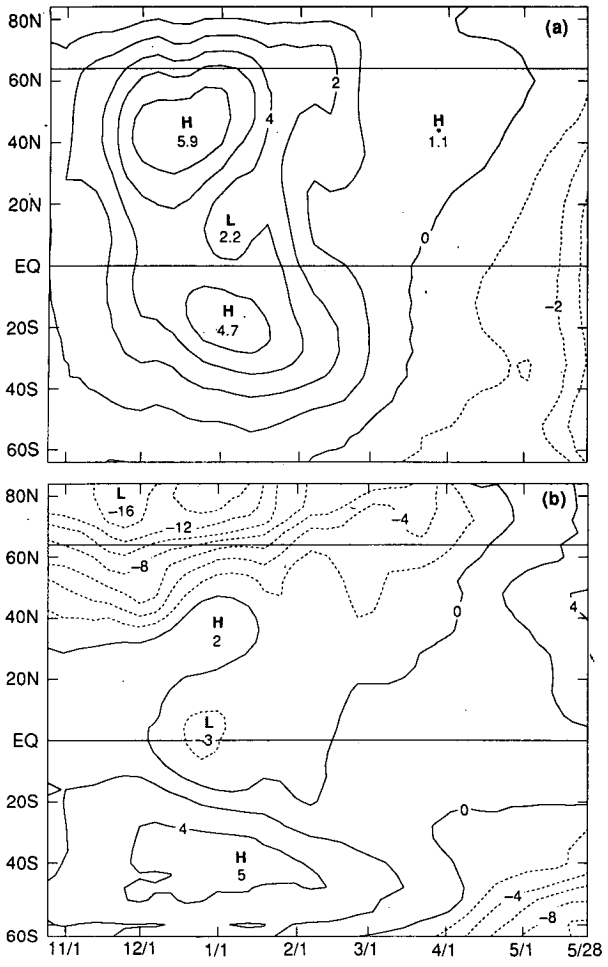

FIG. 7. Latitude–time sections of (a) $\bar{v}^*$, contour interval 1 m s^{-1}, and (b) $\bar{Q}$, contour interval 2 K day^{-1} at 0.1 mb for the LIMS data record.

and more persistent over the South Pole (Figs. 2 and 3). This could be due, in part, to a local circulation caused by enhanced gravity wave sources over Antarctica relative to the circumpolar ocean. It could also be due to differences in the upward transmissivity of gravity waves. Another puzzle is the observed descent of the separated stratopause with time. It may be that wave–mean flow interaction is such that the westerly jet and region of easterly gravity wave driving migrate downward together, in a fashion similar to that shown by Hartmann et al. (1984) for Rossby wave driving. In section 6 we investigate some of these possibilities with the 2-D model.

6. Numerical simulation

a. *The BISA/NCAR 2-D model*

This radiative-chemical-dynamical model was designed at the Belgian Institute for Space Aeronomy (BISA) and further developed at the National Center for Atmospheric Research (NCAR). The model extends from 85°S to 85°N and the surface to 85 km with resolutions of 5° in latitude and 1 km in altitude. With ≈40 chemical trace species, radiation, and wave–mean flow dynamics, this model is fully interactive, allowing for many types of feedback studies. Chemical species and entropy are advected by a residual (transformed Eulerian) mean meridional circulation in log pressure coordinates, which is forced by spatial gradients in wave driving and radiative heating or cooling. Infrared transfer may be calculated with a detailed accurate algorithm or by Newtonian cooling. For the purposes of this study we use the faster Newtonian algorithm. Further details of the model may be found in Hitchman and Brasseur (1988), in which a new parameterization of Rossby waves was introduced to provide a self-consistent determination of their torque on the zonal flow and dispersion of tracers. In this study we do not use the Rossby wave parameterization. Brasseur and Hitchman (1987) describe the gravity-wave parameterization used in the model. In (3) z_b varies substantially with trace speed. When $\tilde{u}$ also varies with c, z_b varies much more for different trace speeds, leading to undesirably large gradients in wave driving on the flanks of zonal jets in the model. The parameters used in the model are as in Table 1, except we set $\tilde{u}$ = 3 m s^{-1} for all five zonal trace speeds.

We will compare two 5 yr integrations. In run 1, the gravity wave parameterization is not used. No friction or diffusion is applied to the zonal momentum equation (as embodied in the meridional streamfunction equation). A global mean profile of constant vertical eddy diffusivity (K_{zz}) is applied to the temperature and constituent equations. This profile is similar to the global mean of K_{zz} obtained from the gravity-wave breaking parameterization. In run 2 the L/H parameterization is employed, providing the zonal body force and K_{zz} due to breaking gravity waves.

To test the hypothesis that the latitudinal variation in zonal mean, gravity wave source strength near Antarctica could enhance the southern separated stratopause, we made a third run in which A was doubled in the latitude band 85°–65°S. Otherwise, parameters for run 3 were the same as in run 2.

b. *Results*

We are beginning to investigate some of the fundamental causes of the evolution of the basic state with the BISA/NCAR 2-D model. It would be best to use a detailed radiative code to estimate radiative equilibrium temperatures, and determine departures due to gravity-wave driven meridional motions. As an initial calculation, however, we employ the Newtonian cooling approximation to the infrared transfer, and relax toward the initial (22 June) global mean temperature profile at the rate

$$\alpha(z) = 0.0864 \cdot \left[1.5 + \tanh\left(\frac{z-36}{7}\right)\right], \quad (6)$$

where z in km gives a damping rate in day^{-1}. Damping time scales range from ~22 days near the tropopause to ~5 days in the upper mesosphere. These rates are similar to those calculated by Gille and Lyjak (1986) for an infinite vertical wavelength. We chose not to relax toward a seasonally varying climatological cross section, because such values include the very effects of gravity wave driving which we wish to test. Indeed, Fels (1987) shows polar night radiative equilibrium temperatures in the mesosphere to be ~100 K cooler than are observed. Relaxing toward a global mean profile allows the effects of gravity waves to be diagnosed.

Figure 8 shows the body force due to gravity waves, together with the meridional circulation for 28 May in the 5th yr of run 2 (cf. separated stratopause structure for June 1975 and May 1979 in Figs. 2 and 3). The strong easterly acceleration at the top of the winter jet is balanced by poleward flow, with downwelling poleward of 50°S exceeding 1 cm s^{-1} and penetrating below the stratopause. In run 1, where there was no gravity wave driving or friction of any kind, $|\bar{v}^*| < 0.4$ m s^{-1} everywhere (not shown). Thus, gravity wave driving increases the speed of the mesospheric meridional circulation by an order of magnitude.

In run 1 near 60 km, winter westerlies are stronger and appear earlier than summer easterlies (not shown), reflecting the seasonal difference in radiative drive. This leads to a hemispheric difference in mesospheric wave driving, as seen in Fig. 8a. The maximum in $\bar{v}^*$ (Fig. 8b) is located near the maximum in $|DF_g|$. This strong poleward flow gathers and descends in a region confined poleward of ~55°S (Fig. 8c), the latitude of maximum $|DF_g|$.

The temperature difference between runs 1 and 2 is shown in Fig. 9. The winter polar middle atmosphere is much warmer with the gravity wave driven descent. Near 60 km, 85°S the maximum temperature departure exceeds 18 K. The pattern is rather similar to the observed separated stratopause in its confinement to the pole, deep layer of substantial equatorward temperature decrease, and maximization near 60 km in early winter. Although they did not focus on this feature, Holton (1983) and Garcia and Solomon (1985) obtained similar patterns in their models, which contain the L/H parameterization.

We expected that gravity wave driven upwelling over the summer pole would cause that region to be cooler in run 2 than run 1. Instead, Fig. 9 shows that in May the North Pole is also warmer with gravity wave driving than without! At first we thought that the explanation lay in a redistribution of radiatively active species. The gravity-wave driven circulation causes stronger upward motion in the tropics (note positive values in the tropics in Fig. 8c), which results in more ozone at upper levels in run 2. However, the difference in solar heating rate

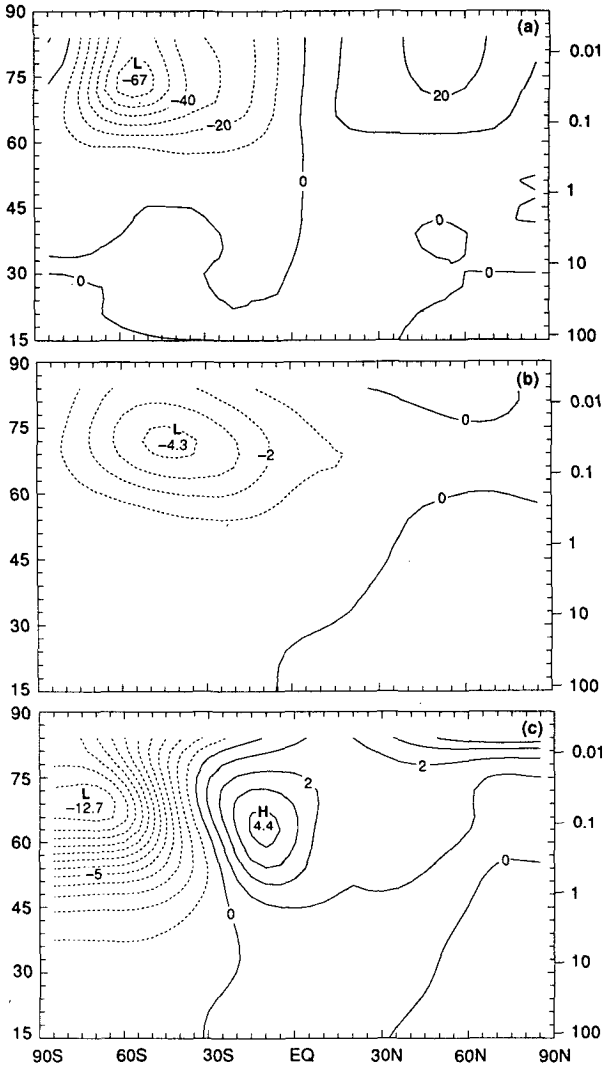

FIG. 8. Latitude–height sections of zonal mean (a) body force due to gravity wave absorption, contour interval 10 m s^{-1} day^{-1}; (b) $\bar{v}^*$, contour interval 1 m s^{-1}, and (c) $\bar{w}^*$, contour interval 2.5 mm s^{-1}, for 28 May on the 5th year of run 2 using the BISA/NCAR 2-D model.

between runs 1 and 2 is not substantial. It turns out that the influence of gravity waves on the model mean flow lasts through winter into late spring. This can be seen in Fig. 10, which shows time–height sections of the temperature difference between runs 1 and 2 at 75°N and 75°S for one year. In each of these two model runs, interannual variability is negligible, so we show only the Fifth year of integration. At 75°N (Fig. 10a), gravity-wave driven downwelling and warming begins in late September. Maximum temperature departures from run 1 are reached by the winter solstice, and persist until the spring equinox, when the perturbation begins to decrease in amplitude. There is still some noticeable effect in May, giving the apparently paradoxical result seen in Fig. 9. Relative cooling associated

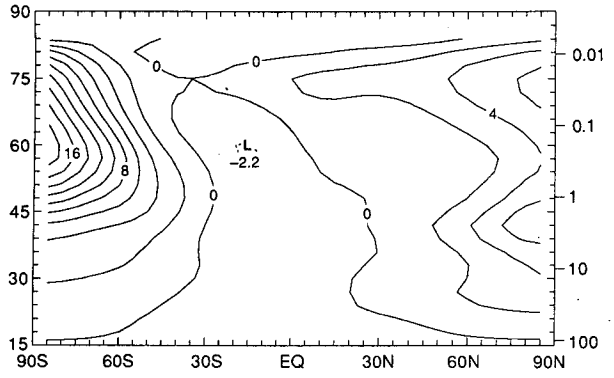

FIG. 9. As in Fig. 8, except of the temperature difference between runs 1 and 2 (run 2 − run 1), contour interval 2 K.

with gravity wave driven upwelling is seen in late summer and fall. At high latitudes, gravity wave driven winter heating dominates over summer cooling in run 2 because of the asymmetry in strength between the winter westerlies and summer easterlies and the strong dependence of gravity wave driving on zonal wind speed. A similar seasonal evolution is seen over the South Pole (Fig. 10b). As in the observations (Fig. 2), large temperature deviations persist through October.

The model results suggest that gravity wave driving increases polar temperatures near 60 km from fall through late spring.

Although the model simulations depart from reality in many details, they can be used to assess the relevance of physical mechanisms. Figure 11 shows the seasonal evolution of temperature at 75°S separately for runs 1 and 2, where the time mean profile was removed in each to emphasize temporal variations. One sees the warm summer stratosphere and the cold winter stratosphere in both panels. An out-of-phase relationship between the stratosphere and upper mesosphere is evident in both, but the node is lower in run 2 (~60 km vs ~72 km). In run 1, with no wave driving, upper mesospheric temperatures *increased* approaching the southern winter (April and May in Fig. 11a). The circulation driven by the changing solar zenith angle alone causes a reversed meridional temperature gradient above 72 km! Stronger solar driven upwelling near the summer stratopause extends upward into the mesosphere in run 1, overcoming the weaker local solar heating to produce temperature decreases. Garcia (1987) showed that when mechanical dissipation is very weak (the wave drag is zero in run 1) the motions induced by local heating can extend upward quite far. With gravity wave driving (Fig. 11b), this summer up-

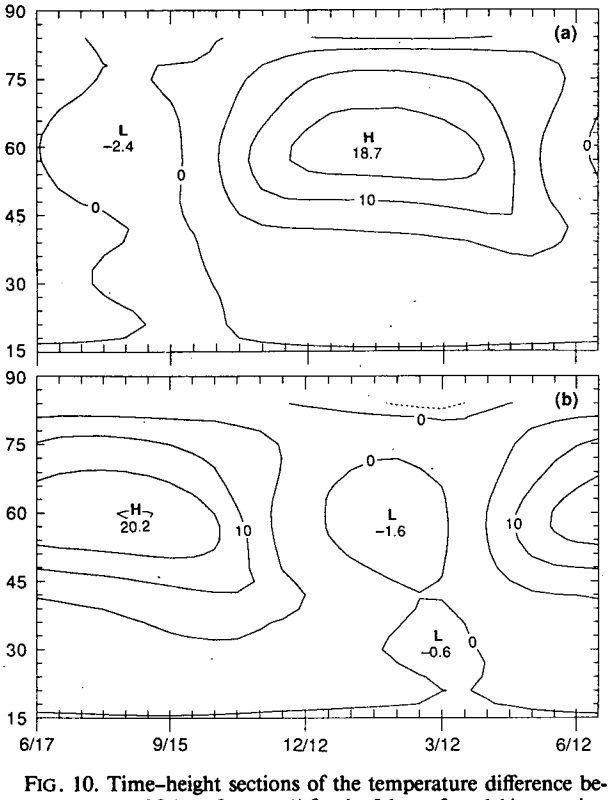

FIG. 10. Time–height sections of the temperature difference between runs 1 and 2 (run 2 − run 1) for the 5th yr of model integration at (a) 75°N, and (b) 75°S. Values at 70°, 75°, and 80° are averaged together before contouring, with an interval of 5 K. Tick marks are spaced 15 days apart.

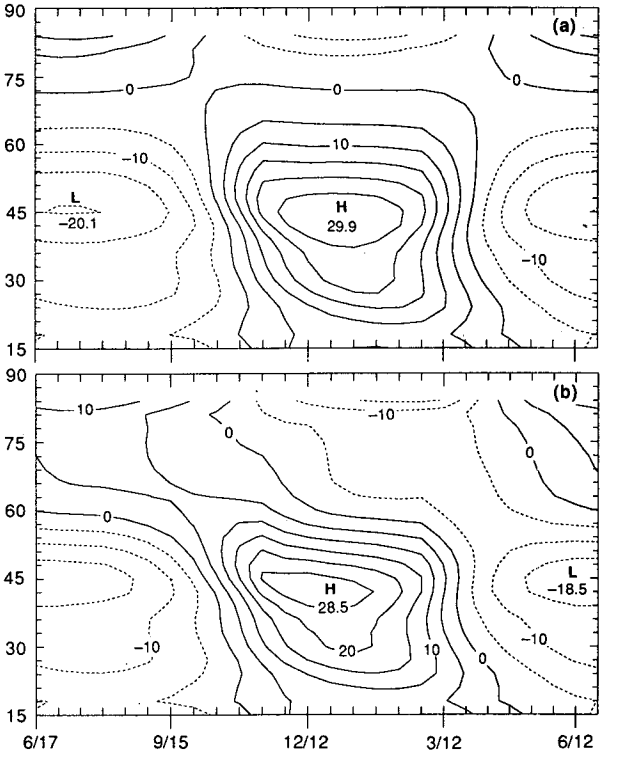

FIG. 11. Time–height sections of temperature at 75°S for the 5th yr of model integration for (a) run 1, and (b) run 2. The time mean profile of each section has been subtracted out. The contour interval is 5 K.

welling and winter downwelling in the mesosphere is greatly enhanced, with the reversed meridional gradient occurring at all levels above 60 km. The altitude above which vertical motions control temperature trends is two scale heights lower in run 2 than in run 1.

In the absence of gravity wave driving, the summer sunlit stratopause descends from ~55 to ~45 km during October and November (Fig. 11a). This is purely a photochemical effect due to the changing solar zenith angle. In run 2, the gravity wave driven winter stratopause descends with time from ~75 km in May until it blends with the radiatively driven summer strato pause near 50 km in November (cf. Fig. 2). In May, strong easterly wave drag (Fig. 8a) closes the westerly jet (not shown). This easterly acceleration causes the level of maximum westerlies to descend, which, in turn, causes the level of maximum easterly wave drag to descend. By this nonlinear wave–mean flow interaction process, the accelerated meridional flow and polar downwelling occur at progressively lower and lower altitudes.

In run 3 gravity wave driving was doubled at and south of 65°S. One would expect enhanced easterly wave driving relative to run 2 in the south polar mesosphere during winter; relative poleward flow, enhanced downwelling over the pole; and upwelling near 50°S. This did cause increased temperatures near 50 km over the pole and relative upwelling in midlatitudes. The differences were small, however, and the pattern was not quite as expected for a local enhancement of the separated stratopause. We conclude that local circulations may be relevant to interhemispheric differences, but the gravity wave source variation is not necessarily the cause. Another component of this problem is gravity wave transmission. The relative lack of planetary Rossby waves in the southern middle atmosphere allows for a more stratospheric wind structure during winter. Gravity wave propagation through the stratosphere is more likely to be the same from week to week and from winter to winter in the Southern Hemisphere. We plan to employ the Rossby wave parameterization to test this hypothesis with the 2-D model, where interhemispheric differences in the upward flux of Rossby wave activity at 15 km are specified from climatology.

7. Conclusions

The polar winter stratopause has a dynamical origin which is quite different from the radiative origin of the sunlit stratopause. Its distinctive shape and temporal behavior lend support to the idea that it is a "separated stratopause." A significant fraction of the stratopause at solstice, the extratropical winter region, is caused by the absorption of small scale waves.

Approaching solstice, the solar heating gradient near the terminator gives rise to a westerly jet which is stronger than the summer easterly jet. As upwelling gravity waves interact with the zontal flow, mesospheric flow from the summer hemisphere to winter hemisphere is greatly strengthened (model results suggest by an order of magnitude). Dynamically driven ascent in the sunlit region is weak, but broad, departures from radiative equilibrium are moderate. Due to spherical geometry, the meridional flow converges over the winter pole, where it descends. The polar confinement of downwelling is due to the relative poleward location of the westerly jet and colocated strong wave driving and induced poleward flow. The intense polar downwelling causes large departures from radiative equilibrium, resulting in a separated stratopause. As the westerly jet and easterly wave drag maxima descend with time, so too does the region of polar downwelling and elevated temperatures. Model results suggest that the effects of gravity wave driven downwelling, which are apparent beginning in fall in the observations, may last into late spring, although they are masked by increasing solar effects in the observations. We speculate that hemispheric differences in the upward transmissivity of gravity wave activity through the stratosphere probably account for hemispheric differences in the behavior of the separated stratopause.

One intriguing model result is that, in the absence of any friction, differential solar heating alone can cause a reversed meridional temperature gradient near the mesopause at solstice. The structure becomes two scale heights deeper with gravity wave driving. But it appears that, contrary to the separated stratopause, the reversed meridional gradient at the mesopause may be partly radiative in origin.

Acknowledgments. We thank Dr. J. Barnett for allowing us to reproduce his figure which first suggested that the South Polar stratopause is anomalously warm in winter. We would also like to thank Cheryl Craig, Larry Lyjak, and Dan Packman for help in data processing, Eric Fetzer, Rolando Garcia and Conway Leovy for useful conversations, and James Holton and Duane Stevens for helpful reviews. This work was supported by the NASA Upper Atmosphere Research Program under Interagency Transfer W16215 and Grant NAGW-1411.

REFERENCES

Bailey, P. L., and J. C. Gille, 1986: Inversion of LIMS radiance measurements; an operational algorithm. *J. Geophys. Res.*, **91**, 2757–2774.

Barnett, J. J., 1974: The mean meridional temperature behavior of the stratosphere from November 1970 to November 1971 derived from measurements by the Selective Chopper Radiometer on Nimbus IV. *Quart. J. Roy. Meteor. Soc.*, **100**, 505–530.

——, and M. Corney, 1985: Middle atmosphere reference model derived from satellite data, *Middle Atmosphere Program, Handbook for MAP*, 16, K. Labitzke, J. J. Barnett, and B. Edwards, Eds., 318 pp.

Brasseur, G., and M. H. Hitchman, 1987: The effect of breaking gravity waves on the distribution of trace species in the middle atmosphere, *Transport Processes in the Middle Atmosphere*, Reidel Publishing, 215–227.

Crane, A. J., 1979: Aspects of the energetics of the upper stratosphere

during the January-February 1973 major sudden warming. *Quart. J. Roy. Meteor. Soc.*, **105**, 185–206.

——, J. D. Haigh, J. A. Pyle and C. F. Rodgers, 1980: Mean meridional circulations of the stratosphere and mesosphere. *Pure Appl. Geophys.*, **118**, 307–328.

Coy, L., and D. C. Fritts, 1988: Gravity wave heat fluxes: A Lagrangian approach. *J. Atmos. Sci.*, **45**, 1770–1780.

Curtis, P. D., J. T. Houghton, G. D. Peskett and C. D. Rodgers, 1974: The pressure modulator radiometer for Nimbus F. *Proc. Roy. Soc. London*, **337A**, 135–150.

Edmon, H. J., B. J. Hoskins and M. E. McIntyre, 1980: Eliassen-Palm cross sections for the troposphere. *J. Atmos. Sci.*, **37**, 2600–2616.

Fels, S. B., 1987: Response of the middle atmosphere to changing ozone and carbon dioxide—A speculative tutorial, *Transport Processes in the Middle Atmosphere*, Reidel Publishing, pp. 371–386.

Garcia, R. R., 1987: On the mean meridional circulation of the middle atmosphere. *J. Atmos. Sci.*, **44**, 3599–3609.

——, and S. Solomon, 1985: The effect of breaking gravity waves on the dynamics and chemical composition of the mesosphere and lower thermosphere. *J. Geophys. Res.*, **90**(D2), 3850–3868.

Gille, J. C., and J. M. Russell III, 1984: The Limb Infrared Monitor of the Stratosphere (LIMS) experiment description, performance, and results. *J. Geophys. Res.*, **89**(D4), 5125–5140.

——, and L. V. Lyjak, 1986: Radiative heating and cooling rates in the middle atmosphere. *J. Atmos. Sci.*, **43**, 2215–2229.

——, L. V. Lyjak and A. K. Smith, 1987: The global residual mean meridional circulation in the middle atmosphere for the northern winter period. *J. Atmos. Sci.*, **44**, 1437–1452.

——, et al., 1984: Validation of temperature retrievals obtained by the Limb Infrared Monitor of the Stratosphere (LIMS) experiment on Nimbus 7. *J. Geophys. Res.*, **89**(D4), 5147–5160.

Hartmann, D. L., C. R. Mechoso and K. Yamazaki, 1984: Observations of wave-mean flow interaction in the Southern Hemisphere. *J. Atmos. Sci.*, **41**, 351–362.

Haurwitz, B., 1961: Frictional effects and the meridional circulation in the mesosphere. *J. Geophys. Res.*, **66**, 2381–2391.

Hirota, I., and J. J. Barnett, 1977: Planetary waves in the winter mesosphere—preliminary analysis of Nimbus 6 PMR results. *Quart. J. Roy. Meteor. Soc.*, **103**, 487–498.

Hitchman, M. H., and C. B. Leovy, 1986: Evolution of the zonal mean state in the equatorial middle atmosphere during October 1978-May 1979. *J. Atmos. Sci.*, **43**, 3159–3176.

——, and C. B. Leovy, 1988: Estimation of the Kelvin wave contribution to the semiannual oscillation. *J. Atmos. Sci.*, **45**, 1462–1475.

——, and G. Brasseur, 1988: Rossby wave activity in a 2-D model: Closure for wave driving and meridional eddy diffusivity. *J. Geophys. Res.*, **93**, 9405–9417.

——, C. B. Leovy, J. C. Gille and P. L. Bailey, 1987: Quasi-stationary zonally asymmetric circulations in the equatorial lower mesosphere. *J. Atmos. Sci.*, **44**, 2219–2236.

Holton, J. R., 1982: The role of gravity wave induced drag and diffusion in the momentum budget of the mesosphere. *J. Atmos. Sci.*, **39**, 791–799.

——, 1983: The influence of gravity wave breaking on the general circulation of the middle atmosphere. *J. Atmos. Sci.*, **40**, 2497–2507.

Houghton, J. T., 1978: The stratosphere and mesosphere. *Quart. J. Roy. Meteor. Soc.*, **104**, 1–29.

Lindzen, R. S., 1981: Turbulence and stress due to gravity wave tidal breakdown. *J. Geophys. Res.*, **86**, 9707–9714.

Pedlosky, J., 1979: *Geophysical Fluid Dynamics*, Springer-Verlag.

Rodgers, C. D., 1976: Retrieval of atmospheric temperature and composition from remote measurements of thermal radiation. *Geophys. Space Phys.*, **14**, 609–624.

Solomon, S., J. T. Kiehl, R. R. Garcia and W. Grose, 1986: Trace transport by the diabatic circulation deduced from satellite observations. *J. Atmos. Sci.*, **43**, 1603–1617.

Wehrbein, W. M., and C. B. Leovy, 1982: An accurate radiative heating and cooling algorithm for use in a dynamical model of the middle atmosphere. *J. Atmos. Sci.*, **39**, 1532–1544.